JET-R(96)04

H/D Measurement by Neutral Particle Analysis at JET

G Bracco[1], KGuenther.

JET Joint Undertaking, Abingdon, Oxfordshire, OX14 3EA, UK.
[1] Associazione EURATOM-ENEA, CRE ENEA Frascati, Via E. Fermi 27, I-00044, Frascati, Italy.

ABSTRACT

The paper describes the measurement of the hydrogen isotope relative concentration by means of the analysis of the emitted flux of neutral particles. The measured flux ratio must be corrected in order to retrieve the proper density ratio, and an approximate conversion function has been derived. A model for the neutral particle emission is described and the results compared with the experiment for ohmic plasma conditions. The H/D behaviour during part of the 1994-1995 campaign is shown. The analysis of the ELM-free phase of hot-ion mode plasmas shows a large increase of the H/D flux ratio which is quenched by the occurrence of a giant Elm. A modified version of the model has been applied to this case in order to assess if the halo neutral density can explain the observation.

I. INTRODUCTION

The experimental determination of the relative concentration of the hydrogen isotope ions (H, D, T) is an important issue in nuclear fusion experiments. In a deuterium plasma, the knowledge of the H/D density ratio is essential for both the evaluation of the absolute deuteron density in the plasma core and the study of the isotope retention in the materials surrounding the plasma. This information is even more crucial in reactor relevant experiments using a DT mixture.

Neutral particle analysis (NPA) consists of the measurement of the energy spectra of neutrals emitted from a plasma. It has been used since the early times of nuclear fusion research to evaluate the ion temperature [1,2,3] in H and D plasmas. More recently NPA has permitted the study of fast ion tails generated by neutral beam injection [4,5], by ion cyclotron [6,7] and lower hybrid [8] radio-frequency heating.

This paper illustrates the application of NPA to the evaluation of the H/D density ratio. The direct experimental data consists of the ratio of H to D neutral particle fluxes which can be converted into the density ratio by using a model for the neutral particle emission. NPA technique has already been used to serve this purpose in the past [3,9,18], together with other methods available (H_α/D_α Balmer α-line ratio, mass spectrometry by a quadrupole analyser), but no attempt has been made so far to convert flux ratios into density ratios. The other techniques are relevant to the H/D measurement at the very edge of the plasma, in the scrape-off region (H_α/D_α) or in the residual gas after the plasma pulse (the quadrupole analyser), while NPA permits access to the plasma core.

This paper briefly describes the neutral particle analyser used at JET, illustrates the model for the neutral particle emission together with some practical formulas which can be used to convert flux ratios into density ratios, and finally reports the experimental results both for ohmic and neutral beam heated discharges.

The data recorded during the ohmic phase of a series of pulses of the 1994-1995 campaign show the evolution of the H/D ratio as a consequence of opening the vessel, air leaks, and a large H_2 injection caused by a test of the pellet injection system.

An interesting increase of the measured H/D flux ratio has been observed during ELM-free H modes in neutral beam heated discharges. The increase appears to be quenched by the arrival of a giant ELM. This phenomenon, not fully understood, is the object of a dedicated simulation attempt.

II. THE DIAGNOSTIC

The neutral particle flux emitted from the JET plasma in the energy range 1.3 to 250 keV is measured by a time of flight neutral particle analyser (TOF-NPA) [10], which is now located near to the equatorial plane of the tokamak and observes the plasma perpendicularly to the toroidal magnetic field (figure 1).

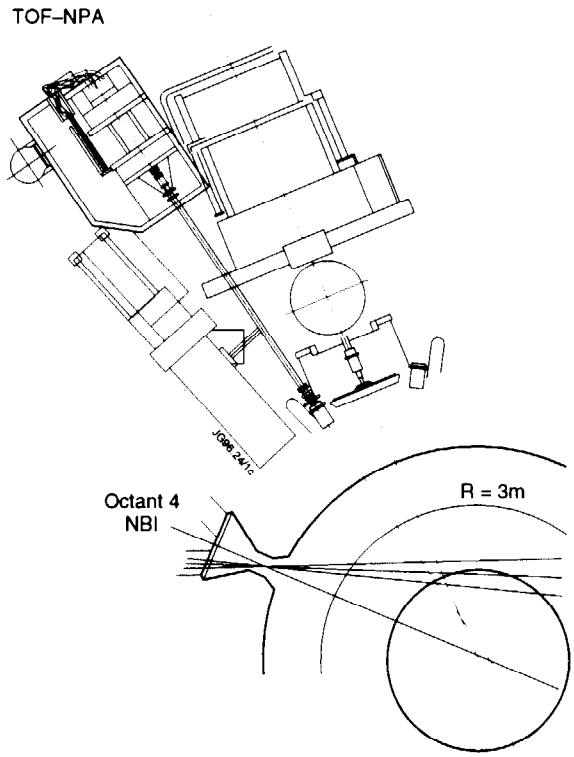

Fig.1: TOF-NPA layout at octant 3 together with neutral beam injection lines at octant 4.

The neutrals coming from the plasma are ionised in a gas stripping cell and energy analysed by a cylindrical electrostatic plate system. A set of 15 TOF detectors collects the ions with an energy dynamic range of 1:28. Each detector consists of a thin carbon foil and two channeltrons. It detects particles by a time coincidence technique. An incoming ion produces secondary electrons in the carbon foil which are detected by the first channeltron (CEM A), thus

providing a start trigger signal. The signal in the second channeltron (CEM B), produced directly by the ion at the end of its flight, constitutes the stop signal. The mass discrimination for particles with the same energy is based on their time of flight (50 to 400 ns according to the channels and to the selected energy) using a correspondingly delayed coincidence time gate τ_G, which can be varied in the range of 5 to 33 ns. The standard analyser settings are: energy range 2.9 to 80 keV for the 15 channels, time gates 15 ns.

The coincidence technique rejects any sort of random events (UV radiation, neutrons) with a residual signal contamination of the order of $C_A C_B \tau_G$ where C_A and C_B are the random noise count rates in CEM A and B, respectively. The good random noise rejection capability makes it possible to reliably measure the extremely low neutral fluxes emitted by an ohmic plasma.

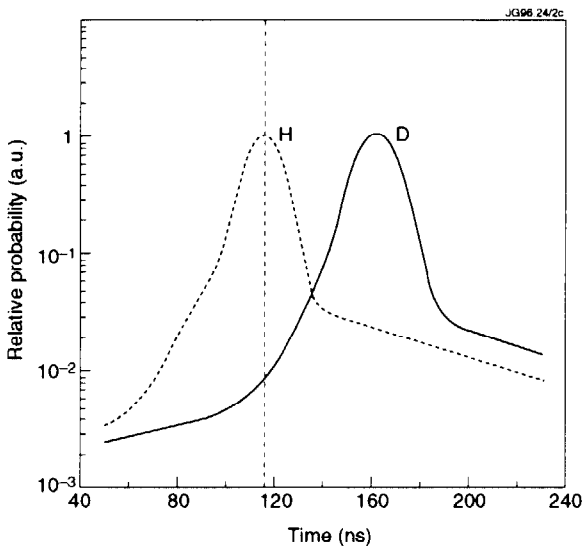

Fig.2: Time distribution for H and D, channel 4 (7.8 keV), coincidence time gate 15 ns.

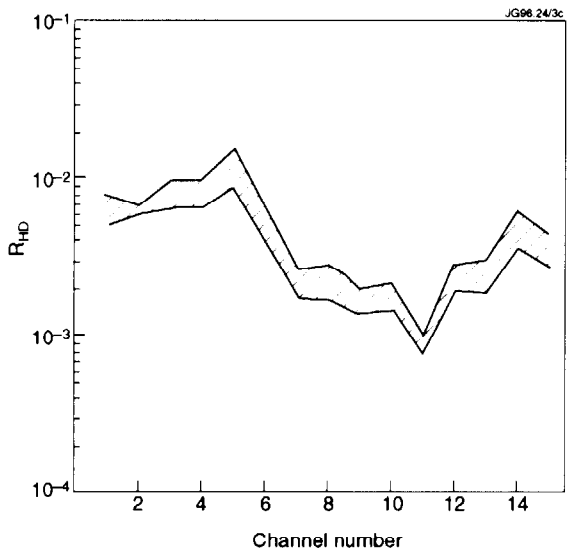

Fig.3: Mass rejection factor R_{HD} versus channel number. The shaded area takes into account ±3 ns of error in the time tuning of the coincidence electronics.

The mass selection capability of the TOF-NPA depends on the distribution of the actual time differences between the start and the stop signals. This distribution is a function of the selected particle, energy, and the characteristics of the selected channel. These time distributions have been measured during the analyser calibration [10] and the results have been empirically interpolated in the range of the setting parameters. Figure 2 shows an example. It can be seen that the rejection factor R_{HD}, which describes the contamination of the H signal by the D one, is less than 1%. In figure 3 the R_{HD} factor is shown as a function of the channel number for the standard setting of the TOF-NPA.

In the present analysis the experimental coincidence count rates C_H and C_D for H and D, respectively, are converted into neutral fluxes, Φ_H and Φ_D , using the following expressions

which take into account the corrections due to both random coincidences and H contamination by D

$$\Phi_D = \frac{C_D - C_A C_B \tau_G}{S\Omega\eta_D\Delta_E} \quad (1)$$

$$\Phi_H = \frac{C_H - C_A C_B \tau_G - R_{HD} C_D}{S\Omega\eta_H\Delta_E} \quad (2)$$

where S and Ω are the observed area and solid angle, respectively, Δ_E is the energy resolution, and η_H, η_D are the analyser efficiencies for H and D which have been measured in the calibration [10]. The equations 1 and 2 are valid [11] for a D plasma with an H minority and for the case when C_A and C_B are dominated by the background noise, which is the case, indeed, if the random coincidence term is important (high neutron production). By using the expressions 1 and 2 it is possible to perform reliable H/D flux measurements down to values of the order of 1%. The fact that C_D and C_H for a given energy are measured by the same TOF module assures that any deterioration of the analyser efficiency has virtually no effect on H/D.

III. A MODEL OF NEUTRAL EMISSION

Inside the plasma the local source $S_m(E)$ of neutrals of the sort m at the energy E due to both charge exchange and recombination is given by

$$S_m(E) = n_m(E) \left(n_0 \langle\sigma v\rangle_{cx} + n_e \langle\sigma v\rangle_{rc} \right) \quad (3)$$

where $n_m(E)$ is the ion density of the detected species m per unit energy and solid angle, n_0 is the neutral density, n_e is the electron density, and $\langle\sigma v\rangle_{cx}$ and $\langle\sigma v\rangle_{rc}$ are the reaction rates for charge exchange and radiative recombination, respectively.

The neutral particle flux, computed as the line-of-sight integral of the particle source, taking into account the neutral attenuation by ionization and charge exchange, reads

$$\Phi_m(E) = \int_0^{s_{max}} S_m(E) \exp(-N_{\lambda_m}) \, ds \quad (4)$$

The integration has to be performed along the full line of sight in the plasma. $N_{\lambda m}$ is the the number of mean free paths for the observed neutral particle, from the emission location to the plasma edge, i.e.

$$N_{\lambda_m}(s) = \int_0^s \frac{1}{\lambda_m} ds' \quad (5)$$

where the neutral mean free path λ_m is given by

$$\lambda_m = \frac{v_m}{n_e \left(\langle\sigma v\rangle_{cx} + \langle\sigma v\rangle_{ii} + \langle\sigma v\rangle_{ei}\right)} \tag{6}$$

$\langle\sigma v\rangle_{ii}$ and $\langle\sigma v\rangle_{ei}$ are the ionization reaction rates for ion and electron collisions, respectively. v_m is the particle velocity corresponding to the energy E. The fact that in equation 6 the electron density multiplies $\langle\sigma v\rangle_{cx}$ as well as $\langle\sigma v\rangle_{ii}$ takes into account somehow the effect of the ionization and charge exchange with impurity ions, as it has been shown [12] that the quantity $\langle\sigma v\rangle_{cx} + \langle\sigma v\rangle_{ii}$ scales roughly with the Z of the impurity ion compared to the hydrogen value.

If the energy distribution of ions is Maxwellian with temperature T_m, we have

$$n_m(E) = \frac{n_m\sqrt{E}}{2\pi^{3/2}T_m^{3/2}}\, e^{-E/T_m} \tag{7}$$

The radial localization of the origin of the emitted neutral flux is determined by a competition of the terms which are peaked at the plasma boundary, n_0 and the attenuation term in equation 4 on the one hand, and the term 7 on the other hand, which for E greater than 1.5 times the peak ion temperature is increasing towards the plasma centre. Since for both factors the radial dependence is exponential but opposite in sign, the effect is a rather well defined localization for each measured energy.

The evaluation of equation 4 requires the profiles of n_e, T_e, n_m, T_m, and n_0. n_e and T_e are routinely provided by other diagnostics (LIDAR, ECE, DCN interferometer), the T_m profile is measured only in the neutral beam heated phases with CXRS (charge exchange recombination spectroscopy), while during ohmic phases some information can be obtained from the DD neutron yield monitors, from an X-ray crystal spectrometer and from the NPA itself, by fitting the slope of the energy spectra. In the model the temperatures of H nd D are assumed to be the same.

No direct measurement of n_0 in the plasma core is available. In order to evaluate n_0, a neutral transport code similar to [13] has been used. The code solves the continuity equation for n_0 in cylindrical geometry by explicitly computing the neutral flux, assuming that neutrals are generated at the local ion temperature by charge exchange and recombination. The solution is found by an iterative method with the influx of cold neutrals as a boundary condition. The latter is given by assigning the edge neutral density $n_0(a)$ and temperature $T_0(a)$ which constitute the free parameters in the simulation, to be determined by the fit of the absolute value of the emitted flux. The code also evaluates the neutral temperature by performing the local average of the neutral energy. As the H fraction is a minority, the entire simulation is performed by assuming a pure D plasma with $n_D = n_e$, so that the dilution due to impurity is not taken into account. This approximation is justified by the fact that the dilution affects mainly the absolute intensity of the

computed neutral flux, which is somehow arbitrary as $n_0(a)$ and $T_0(a)$ are free parameters, but not the source localization in the plasma, owing to the assumption in equation 6. The application of a cylindrical 1-D neutral transport code to the D shaped geometry of JET has been studied in [14] showing that the simple 1-D code can still be used significantly. In the case of neutral injection, which will be discussed later, the neutral density due to the neutral beam halo has also to be considered.

The assumption in equation 7 of a Maxwellian ion energy distribution is not trivial, since the TOF-NPA observes neutrals in a very small solid angle ($4x10^{-8}$ sr) around the direction perpendicular to the tokamak magnetic field. Ions with a very large perpendicular velocity component are either near their banana tips or are trapped in the local ripple of the toroidal field. The two populations are coupled according to the ripple-banana convective transport mechanism [15]. Most of the experimental data concerning the H/D ratio refers to energies lower than 20 keV, because in an ohmic plasma the flux intensity at higher energies is very low, while in additionally heated discharges the ion distribution at higher energies is dominated by fast ion tails [4,5,6,7,8]. As in JET the ripple value is very low (0.1% at the edge) it can be assumed that no strong ripple transport takes place at these low energies, and this is confirmed by preliminary results of the 1995 ripple experiment where the neutral spectra in the ohmic phase do not change during an increase of the ripple of up to 1% at the edge. In conclusion the assumption of a Maxwellian distribution is reasonable if the local velocity distribution is dominated by collisions and no angular-selective source or loss mechanism is present.

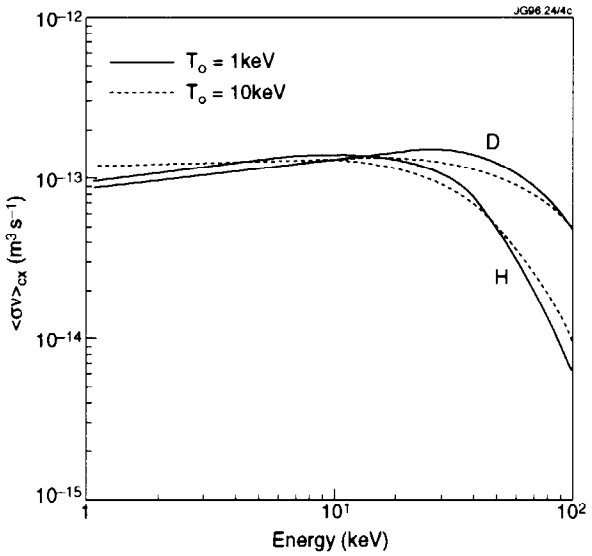

Fig.4: Charge exchange reaction rate $<\sigma v>_{cx}$ versus incident particle energy of H and D ions for neutral temperatures T_0 = 1 and 10 keV.

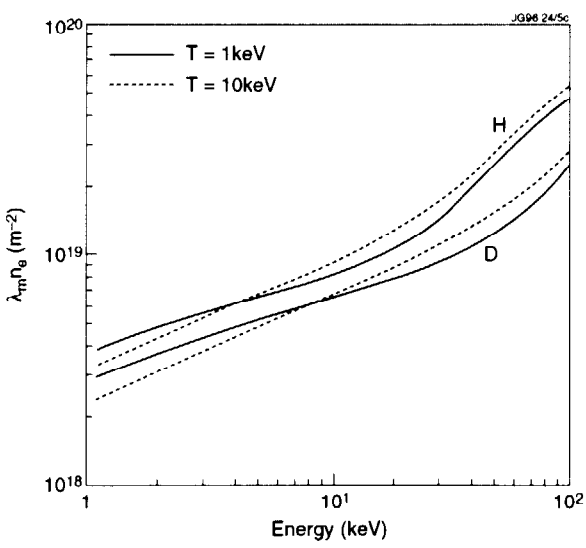

Fig.5: Neutral mean free path parameter, equation 6, for H and D neutrals versus energy for plasma temperatures T = 1 and 10 keV.

The reaction rate coefficients in equations 3 and 6 have been evaluated as the proper integral of the cross sections found in the literature over the plasma or neutral Maxwellian

energy distribution, according to the various cases, and the results have been stored in tables as functions of the particle energy and the target temperature, from which the values used in the simulation are retrieved by interpolation.

The most relevant atomic data are shown in figures 4 and 5, where $<\sigma v>_{cx}$ and the product $\lambda_m n_e$ are plotted versus the particle energy for H and D. It can be seen that the temperature dependence is weak in this energy range and some approximate expressions can be derived, where M_m is the mass of the selected ion species. At energies lower than 20 keV

$$<\sigma v>_{cx} \approx 1.1 \times 10^{-13} \qquad (m^3/s) \qquad (8a)$$

$$\lambda_m \, n_e \approx 3 \times 10^{18} \sqrt{\frac{E}{M_m}} \qquad (m^{-2}, keV, amu) \qquad (9a)$$

while for an energy between 20 and 100 keV

$$<\sigma v>_{cx} \approx 2 \times 10^{-13} \exp\left(-\frac{1}{30}\frac{E}{M_m}\right) \qquad (m^3/s, keV, amu) \qquad (8b)$$

$$\lambda_m \, n_e \approx 1.3 \times 10^{18} \left(\frac{E}{M_m}\right)^{0.8} \qquad (m^{-2}, keV, amu) \qquad (9b)$$

By making use of relation 8a and 9a together with the equations 4 to 7 it is possible to conclude that, at an energy lower than 20 keV, the only mass dependent term in the neutral production equation is the absorption factor in equation 4, so that, if we assume a density ratio n_H/n_D constant in the plasma volume, the flux ratio is

$$\frac{\Phi_H}{\Phi_D} \approx \frac{n_H}{n_D} \exp(1.4 \times 10^{-19} Ln / \sqrt{E}) \qquad (10)$$

where the integration has been replaced by the evaluation of the argument of the integrals at a typical length L, assumed to be the same for H and D. In the JET case, L = 1 m, at E = 10 keV the flux ratio differs from the density ratio by more than 20% for $n > 0.4 \times 10^{19}$ m^{-3} which is a very small density for JET. This demonstrates that generally a correction has to be applied to convert flux ratios into density ratios.

IV. A SEMI-ANALYTICAL APPROACH TO THE MODEL SOLUTION

The model described in the preceding section has been implemented in a computer code, and its results will be shown in the following sections. In order to obtain a practical expression to convert flux ratios into density ratios, a simplified semi-analytical evaluation has been performed. The following assumptions have been made: a radially constant density n, a radially constant density ratio n_H/n_D, a temperature profile as $T(0)(1-(r/a)^2)^\alpha$, where a is the plasma

minor radius, and finally the neutral density is derived only from the balance between ionization and recombination, which is close to the real situation in the core of a high density, low temperature ohmic plasma. In the energy and temperature range between 1 and 20 keV the recombination reaction rate [16] can be approximated by $\langle\sigma v\rangle_{rc} \approx 3.5\text{x}10^{-22}\, T_e^{-1.3}$ (m^3/s, keV) and the total ionization reaction rate by $\langle\sigma v\rangle_{ii}+\langle\sigma v\rangle_{ei} \approx 2\text{x}10^{-14}$ m^3/s, so that

$$n_0 \approx n_i \frac{\langle \sigma v \rangle_{rc}}{\langle \sigma v \rangle_{ii} + \langle \sigma v \rangle_{ei}} = 1.8\text{x}10^{-8}\ n\, T^{-1.3} \tag{11}$$

Using the previous assumptions together with the relations 8a and 9a, the equation 4 can be written as

$$\Phi_m(E) \;=\; 2\text{x}10^{-22}\ n_m\ a\ n\ \sqrt{E}\ [T(0)]^{-2.8}\ e^{-\xi} G(\xi,\mu_m,\alpha) \tag{12}$$

where $\xi = E/T(0)$, and the index m refers to the H and D particles, while the parameter

$$\mu_m = 3.3\text{x}10^{-19}\, a\, n \sqrt{\frac{M_m}{T(0)}} \tag{13}$$

has the physical meaning of the number of mean free paths from the plasma centre to the edge for neutrals at an energy equal to the peak temperature. The function $G(\xi,\mu_m,\alpha)$

$$G(\xi,\mu_m,\alpha) = e^{\xi} \int_0^2 dx\ \frac{\exp\left(-\frac{\mu_m x}{\sqrt{\xi}} - \frac{\xi}{(2x-x^2)^{\alpha}} \right)}{(2x-x^2)^{2.8\alpha}} \tag{14}$$

can be numerically evaluated.

Using equation 12 for the fluxes of H and D, the following relation between flux and density ratios is obtained:

$$\frac{n_H}{n_D} = \frac{\Phi_H}{\Phi_D} \frac{G(\xi,\mu_D,\alpha)}{G(\xi,\mu_D/\sqrt{2},\alpha)} \;=\; \frac{\Phi_H}{\Phi_D} R(\xi,\mu_D,\alpha) \tag{15}$$

For JET ohmic phases the ranges of parameters are: μ_D 2 to 12, ξ 1 to 10, and α 1 to 2. The function $R(\xi,\mu_D,\alpha)$ has been numerically evaluated in this range of parameters and the result has been fitted by the following expression, in which the very weak dependence on ξ has been omitted (units are keV, m, m^{-3})

$$R \approx e^{-0.132 \mu_D^{0.82} \alpha^{0.19}}$$

$$R \approx e^{-1.2\text{x}10^{-16} (an/\sqrt{T(0)})^{0.82} \alpha^{0.19}} \tag{16}$$

Equations 15 and 16 can be used to convert flux ratios into density ratios for ohmic plasmas. The weak dependence on energy, disregarded completely in relation 16, is due to the approximate independence of $\langle\sigma v\rangle_{cx}$ from mass and energy, as shown in relation 8a. The situation would be different at higher energy values, as the relation 8b suggests.

In order to check the assumption made with respect to neutral density, another analytical approach has been chosen, assuming a neutral density profile which decays exponentially from the plasma edge with an e-folding length equal to the mean free path for neutrals at the local ion temperature. With a procedure similar to the one described above, assuming a fixed neutral density at the edge, one obtains a corresponding function $R'(\xi,\mu_D,\alpha)$ which, in the same range of parameters, can be fitted as

$$R' \approx e^{-0.117\mu_D^{0.74}\alpha^{0.40}} \tag{17}$$

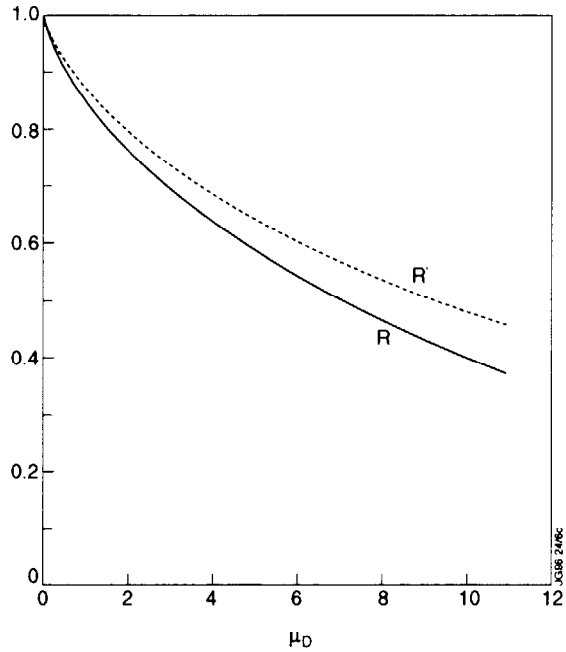

Fig.6: $R(\mu_D,\alpha)$ and $R'(\mu_D,\alpha)$, equations 16 and 17, for α = 1.5 versus μ_D. The functions represent the conversion between flux and density H/D ratios, computed according to two different simplified models.

The parametric dependence is slightly different in equation 17, but the absolute values are similar to the expression 16, as it can be seen in fig. 6 where R and R' are compared for α = 1.5 as a function of μ_D. Hence, the conversion factor of flux into density ratio, H/D, varies between 0.8 and 0.5 in the parameter range typical for ohmic discharges, becoming smaller for high density, low temperature plasmas. As in this approach the conversion factor R is based on the different attenuation between H and D, it can be concluded that whenever the source functions are localized near the edge (e.g., high edge temperature) R must be close to 1.

V. MODEL APPLICATION TO OHMIC PLASMAS

The code, developed on the basis of the model described in the previous sections, performs the line integration according to equation 4, assuming cylindrical geometry and using n_e and T_e profile fits of the LIDAR data. The T_i peak value is obtained from the slope of the neutral spectra and n_H/n_D is assumed to be radially constant.

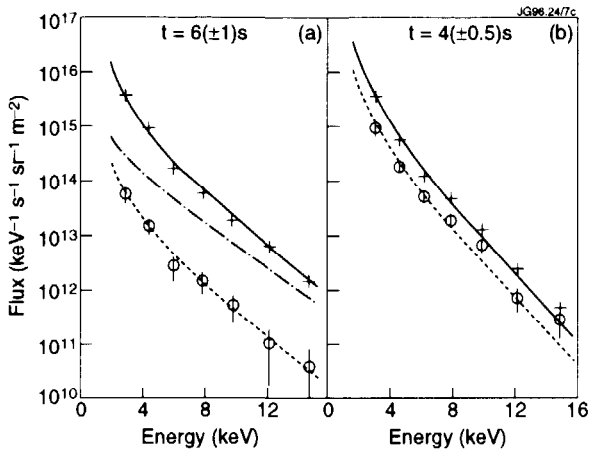

Fig.7: H and D spectra for pulses (a) 32924, Ip = 3 MA, B_T = 3.5 T, and (b) 32712, Ip = 2.5 MA, B_T = 2.8 T. The full and the dotted lines show the simulation results for D and H, respectively, with H/D density ratio equal to 1.1% (a) and 20% (b). The dashed-dotted line displays the D-spectrum resulting from the recombination-only neutral density, equation 11.

The results for the ohmic phases of two pulses, 32924 and 32712, are shown in figure 7(a,b) together with the experimental spectra for H and D neutrals. In pulse 32924 the H/D density ratio is very low, near to 1%, while in the other one H_2 has been injected from the beginning of the pulse and the hydrogen fraction is about 20%. In figure 7(a) the D spectrum evaluated by the approximate approach described in the previous section, taking into account only the recombination $n_{(0)}$, is also shown.

The radial profiles for the pulse 32924 are shown in figures 8 and 9. In the simulation $T_0(a)$ = 50 eV has been chosen and $n_0(a) = 8 \times 10^{15}$ m^{-3} provides the fit of the D spectrum. In figure 9 the case of $T_0(a)$ = 3 eV is also shown to demonstrate that, although a higher $n_0(a)$ value has to be used, the n_0 profile in the inner part of the plasma does not change significantly. Concerning the recombination, in figure 9 two n_0 profiles are plotted: the first is computed using the actual n_e profile and it illustrates the recombination contribution to the total n_0 which attains 60% at the plasma centre; the second one has been computed with the assumption of a constant plasma density, as in the approximate approach of the previous section, and its radial behaviour deviates less from the total n_0 profile than the true recombination contribution.

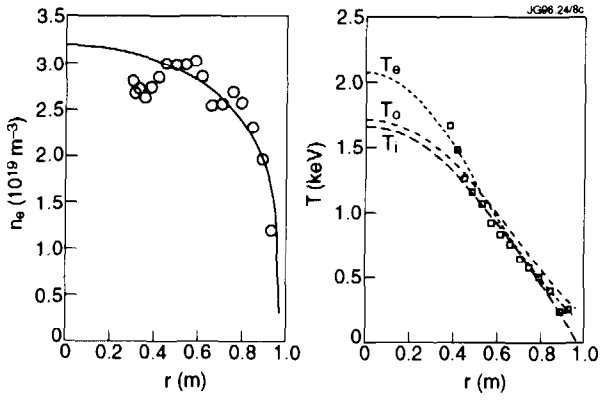

Fig.8: Pulse 32924, t = 6 s; (a) density profile and (b) ion, neutral, and electron temperature profiles used in the simulation, with LIDAR experimental results for n_e and T_e.

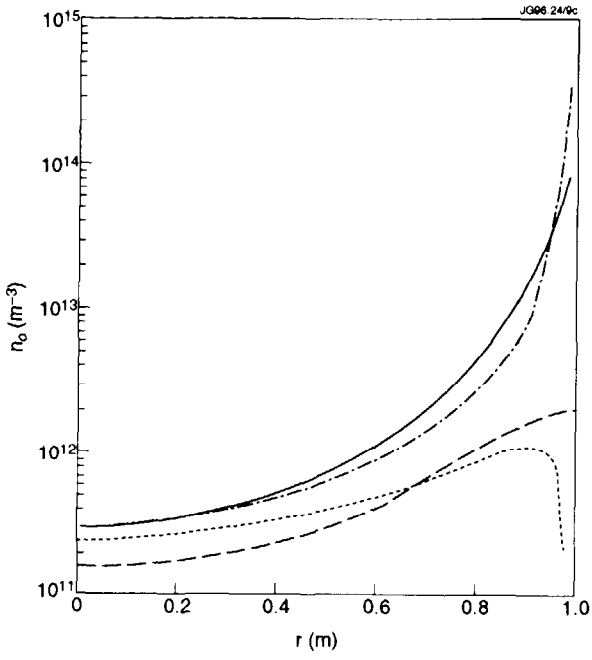

Fig.9: Pulse 32924, t = 6 s; neutral density profiles: full line $T_0(a)$ = 50 eV, dashed-dotted line $T_0(a)$ = 3 eV, (.....) recombination only, (— —) recombination only and constant density profile.

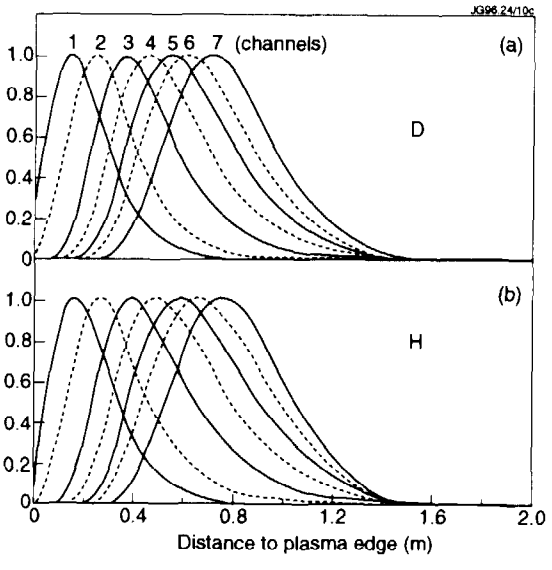

Fig.10: Pulse 32924, t = 6 s; neutral particle source functions for D (a) and H (b), channels 1 to 7 (2.9, 4.4, 6.0, 7.8, 9.7, 11.9, and 14.5 keV), normalized to their maximua.

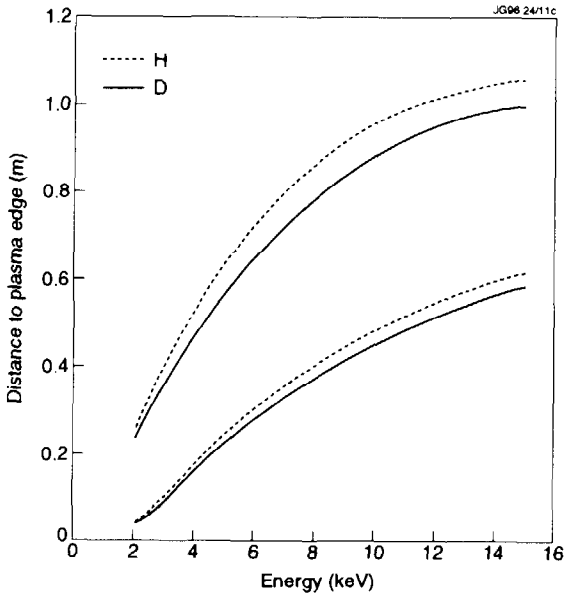

Fig.11: Pulse 32924, t = 6 s; extent of the neutral particle source (limits of the region that produces 2/3 of the flux) for D (solid lines) and H (broken lines) in dependence on energy.

Figure 10 visualizes the localization of the neutral emission. The function which is the argument of the integral in equation 4 is shown, normalized to its maximum, for each of the experimental energies. In figure 11 the distances from the edge at which the integral 4 attains 1/6 and 5/6 of its total value are shown for H and D, as a function of the energy, so that the region where 2/3 of the emission is localized can be identified. H sources are only slightly shifted toward the core.

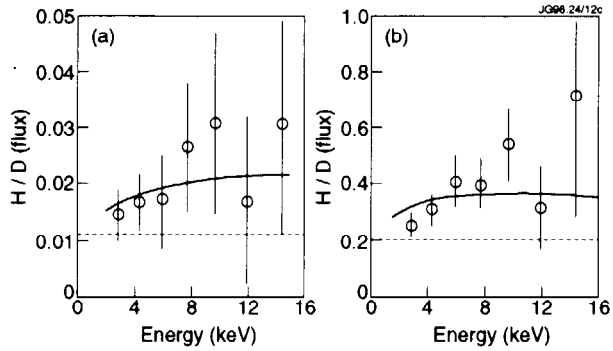

Fig.12: Experimental H/D flux ratio versus energy for pulses 32924, t = 6 s (a), and 32712, t = 4 s (b). The full line is the model result and the dotted line is the H/D density ratio.

In figure 12(a,b) the computed and experimental values of the flux ratios Φ_H/Φ_D are plotted versus energy for the pulses 32924 and 32712. The dotted lines mark the values of n_H/n_D which provide the fit of the H spectra. In both cases the parameters for equations 16 and 17 are $\alpha \approx 1.5$ and $\mu_D \approx 8$, so that the expected conversion factor is $R \approx 0.5$ in good agreement with the results of the full simulation.

The issue of a radial variation of the n_H/n_D ratio can be discussed at this point. From figures 10 and 11 it can be seen that emission regions are rather wide, 0.3 to 0.6 m, and overlap largely for the different energy channels. From figure 12(a,b) it can be concluded that the assumption of no radial variation of n_H/n_D is in agreement with the experimental results. In fact, due to the overlap of the emission regions at different energies, only large radial variations of the n_H/n_D ratio between the plasma centre and the edge could produce a relevant effect on the flux ratios as a function of energy.

VI. LONG TERM MONITORING OFTHE H/D RELATIVE CONCENTRATION IN OHMIC PLASMAS.

The TOF-NPA signal can be used to monitor the relative H/D concentration during the various operation periods of the tokamak. In figure 13(a,b), both Φ_H/Φ_D (a) and n_H/n_D (b), obtained by the approximate relation 16, are shown as functions of the pulse number for the pulse range 32600-34200, corresponding to most of the campaign from the end of November 1994 to the beginning of March 1995. The measurement has been performed with channel number 4 of the

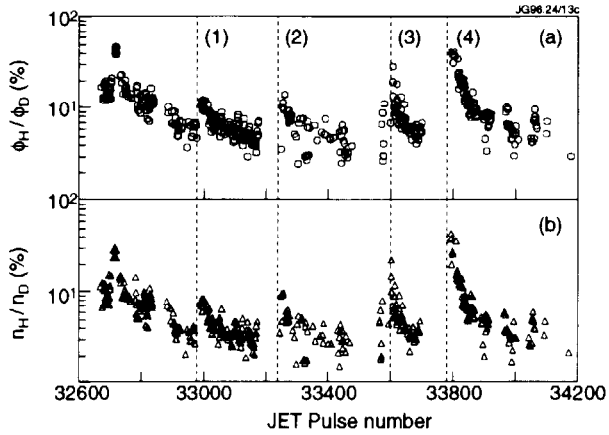

Fig.13: Experimental H/D flux ratio (a) and density ratio (b) for pulses in the range 32650 to 34200 as a function of the pulse number; data during the ohmic phase at 6 s. The vertical lines indicate: (1) air leak, (2) Christmas shutdown, (3) H_2 injection from pellet system, (4) February shutdown. The filled symbols near pulse 32700 relate to pulses with H_2 injection.

TOF-NPA, 7.8 keV for the standard setting of the analyser, at t = 6 s during the ohmic phase. The data collection has begun about 100 pulses after the start of plasma operation following the November 1994 shutdown. n_H/n_D is about 10% and decreases slowly down to a few percents. In this period the H_2 gas injection experiment can be identified. n_H/n_D increases again to 8% after an air leak on December 11, 1994, before pulse 32988. The following increases correspond to the Christmas shutdown, before pulse 33240, to a large injection of the H_2 gas used as a propellant for the pellet system, before pulse 33607, and finally to the opening of the vessel at the beginning of February 1995, before pulse 33800.

VII. H/D INCREASE DURING NEUTRAL BEAM INJECTION IN ELM-FREE H MODES

The evaluation of the H/D ratio using neutral particle emission is a delicate task during additional heating both with NBI and ICRH since neutral spectra can be dominated either by slowing down ions or by fast ion tails [4,5,6,7].

An attempt of analysis has been made to study the observation of a large variation of the H/D ratio at low neutral energy, in coincidence with the giant ELMs at the end of the ELM-free hot-ion H mode phase [17] of a NB heated plasma. Figure 14 shows the neutral beam power, the D_α intensity, the D-D neutron reaction rate, the LIDAR volume averaged density and the H/D flux ratios for the low energy channels, for pulse 32924. It can be seen that the H/D flux ratio first increases up to 10%÷15% at the beginning of the beam phase followed by a gradual increase to about 35% at t = 13 s, with a reduced augmentation in channel 1. The occurrence of the ELM, at t = 13.193 s, restores a low value of H/D for all the channels. In figure 15 the

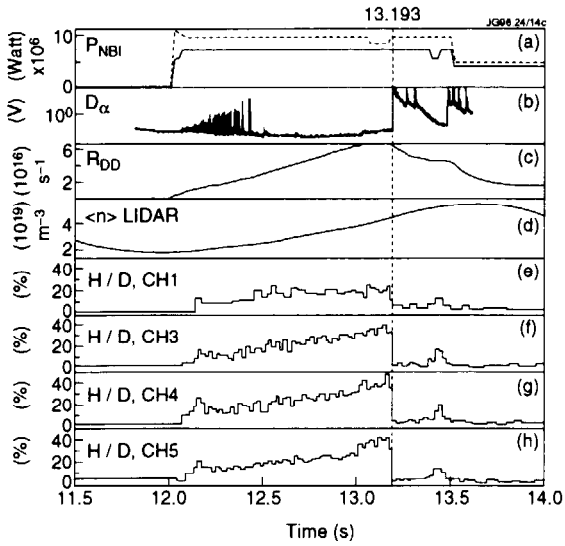

Fig.14: Pulse 32924; time traces of (a) neutral beam power (—) octant 8, 140 keV, (– –) octant 4, 80 keV, (b) D_α (c) D-D reaction rate, (d) LIDAR volume averaged density, H/D flux ratios at 2.9 keV (e), 6.0 keV (f), 7.8 keV (g), and 9.7 keV (h).

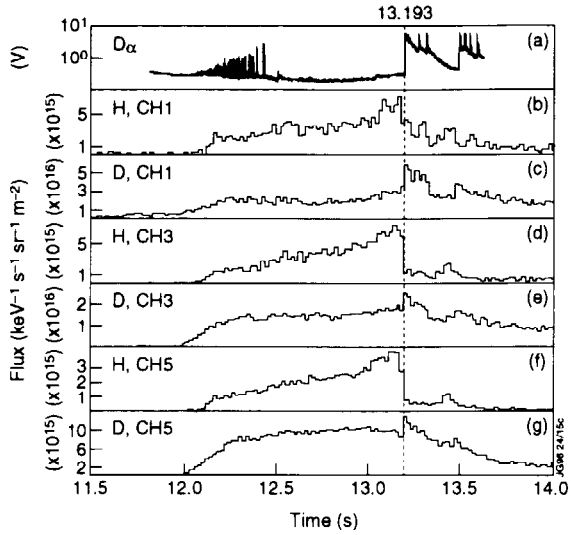

Fig.15: Pulse 32924; time traces of (a) D_α, H and D fluxes at 2.9 keV (b,c), 6.0 keV (d,e), and 9.7 keV (f,g).

corresponding H and D fluxes are shown to demonstrate that the D fluxes increase slightly at the time of the ELM while the H fluxes decrease drastically. In figure 16 the fluxes in the H and D high energy channels are shown. Obviously, in this energy range the D signal is dominated by the slowing down ions, while the H signal is due to the thermal contribution which increases with the increasing ion temperature, see figure 14(c). Also at these high energies a decrease stronger for the H flux than for the D one is seen coincidently with the ELM, with a reduced effect at 80 keV. The variation of the signal happens in a time interval equal to or shorter than one count cumulation time of 20 ms.

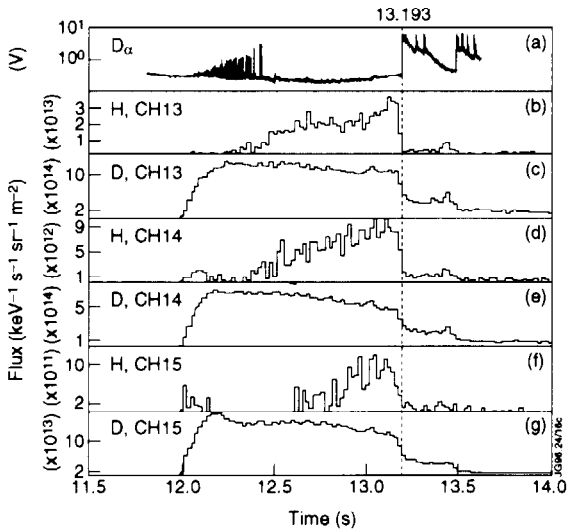

Fig.16: Pulse 32924; time traces of (a) D_α, H and D fluxes at 44 keV (b,c), 57 keV (d,e), and 80 keV (f,g).

If the variation of the H/D flux ratio reflects a genuine variation of the H content in the plasma core, the increase of the H fraction would be of great relevance for the interpretation of the D-D neutron yield. However, the fast decrease of the H/D ratio triggered by the ELM could imply that the increase of the H/D density ratio during the ELM-free phase is restricted to a

reduced plasma volume corresponding to the high confinement region characteristic of the H mode, which is destroyed by the ELM, so that the subsequent efflux of particles from the plasma core restores the H/D ratio typical of the inner part of the plasma. Even this picture of a H/D increase in a limited plasma region would be of interest for the analysis of the particle transport in H mode plasmas.

The physical understanding of the phenomenon is difficult due to the complicate experimental situation for the neutral flux measurement when the neutral beam injection systems are used. In JET there are two NBI systems, 140 keV and 80 keV. Each system consists of 8 neutral beams arranged in two vertical arrays of 4 beams each, having two different angles with the toroidal magnetic field (tangential and normal arrays). The four neutral beams in each of the vertical arrays are symmetrically positioned in respect to the equatorial plane. The TOF-NPA line of sight intercepts the plane of the 80 keV tangential beams in the inner part of the torus, figure 1, at about 0.8 m inwards from the plasma centre. The transverse extent of each neutral beam is of the order of 0.4 m at that location and the vertical extent of the array of 4 beams is about ±0.35 m relative to the equatorial plane.

In these conditions the neutral beams may contribute to the emitted neutral flux by charge exchange between plasma ions and the total neutral density due to the beams and the beam halo (the neutrals created around the beam by charge exchange). It has been shown in sections III and IV that the conversion between the H/D flux ratio and the density ratio depends on the location of the neutral sources in the plasma, so that a variation of the source position, caused by the beam induced neutral density, can modify, in principle, the measured H/D flux ratio. The occurrence of an ELM produces a large increase of electron density at the plasma edge, so that both beam attenuation and the halo can be influenced, with an overall reduction of the beam induced neutral density. Even if the neutral beam itself is the cause of the increase of the H/D flux ratio, the plasma conditions typical of the ELM-free H mode must still play a role since the slow increase of the ratio is observed systematically only in this situation, while it is absent in L modes or in ELMy H modes. Unfortunately, no case of an ELM-free H mode with only the 140 keV beams has been obtained so far, as this would rule out a direct contribution of the 80 keV beam to the TOF-NPA signal. In the case of pulse 33642, the sources number 7 and 8 at 80 keV, the nearest ones to the TOF-NPA view line, have been switched off at the same time as the sources at 140 keV, before the end of an ELM-free H mode, and a simultaneous drop of the H/D flux ratio has been observed (figure 17). In this case the variation of the H and D fluxes is reduced in comparison to the giant ELM case, figure 15, but can clearly be observed (figure 18). Even if the case of pulse 33642 seems to indicate a direct effect of the beam on the H/D flux ratio, a quantitative analysis is required to assess if the halo by itself can account for the observed phenomena.

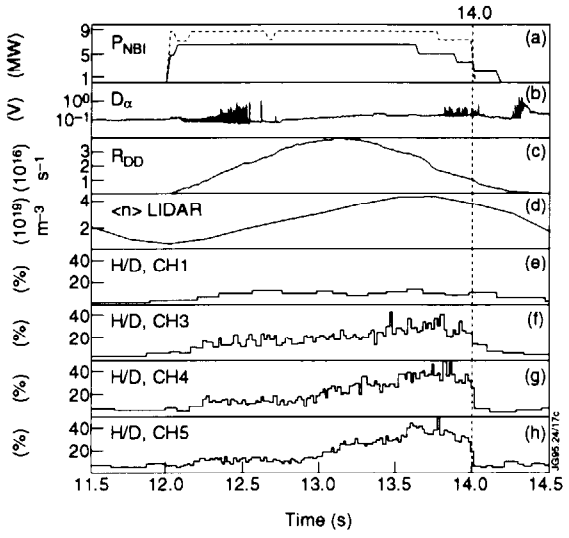

Fig.17: Pulse 33642; time traces of (a) neutral beam power (—) octant 8, 140 keV, (– –) octant 4, 80 keV, (b) D_α, (c) D-D reaction rate, (d) LIDAR volume averaged density, H/D flux ratios at 2.9 keV (e), 6.0 keV (f), 7.8 keV (g), and 9.7 keV (h).

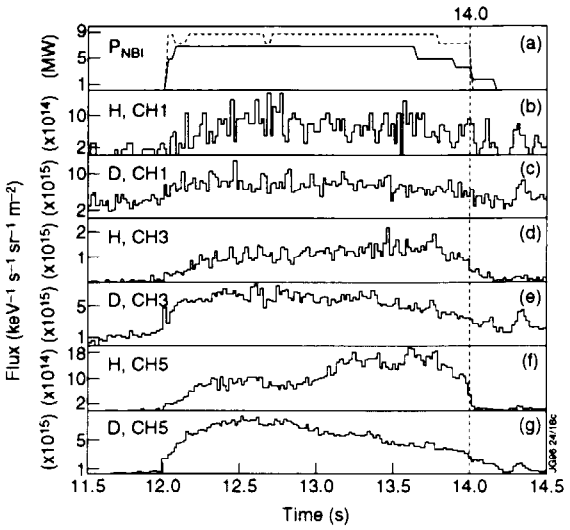

Fig.18: Pulse 33642; time traces of (a) neutral beam power (—) octant 8, 140 keV, (– –) octant 4, 80 keV, H and D fluxes at 2.9 keV (b,c), 6.0 keV (d,e), and 9.7 keV (f,g).

VIII. A MODEL FOR THE H NEUTRAL EMISSION DURING D NEUTRAL BEAM INJECTION

The model described in section III has been extended to allow the analysis of the neutral beam injection phase by taking into account the neutral density of the beam and of its halo. Only the thermal part of the spectra has been modelled, without any attempt to simulate the slowing down ion energy distribution.

It is the purpose of this section to assess if the halo can be the origin of the observed phenomena, but the modelling is not accurate enough to perform a detailed quantitative analysis.

The halo neutral density has been evaluated using a code similar to the one described in section III to calculate the neutral density in the plasma. The code assumes cylindrical geometry around the neutral beam axis and uniform plasma parameters in the direction perpendicular to the beam. The halo density is evaluated using the neutral beam density as a source, taking into account the attenuation of the beam through the plasma. A simplified neutral beam geometry is used, assuming a single beam line in the equatorial plane with the proper toroidal angle (figure 1). The beam power has to be regarded as an adjustable parameter to control the halo intensity. The halo neutral density has been added to the plasma neutral density, evaluated as before, to obtain the estimate of n_0 that enters the neutral source term according to equation 3.

The spectra measured at three times of the pulse 32924 have been analysed, making use of LIDAR and CXRS data. The first is at t = 13 s, just before the giant ELM, i.e. at the maximum of the H/D flux ratio. The second is at t = 13.3 s, just after the giant ELM, when the

H/D flux ratio has dropped by a factor larger than 5, and the third is at t = 12.1 s, at the very beginning of the neutral injection phase. The purpose is to assess if the change in the plasma profiles between t = 13 s and t = 13.3 s, combined with the halo effect, can explain the variation of the H/D ratio. The example at t = 12.1 s is to illustrate the halo effect in a plasma with a much lower density.

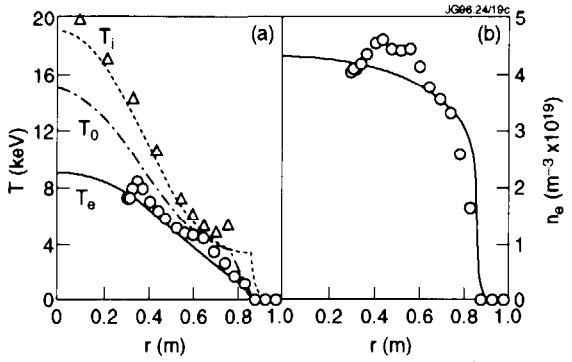

Fig.19: Pulse 32924, t = 13 s; profiles used in the simulation, (a) T_e, T_i, and T_0 (O LIDAR and Δ CXRS), and (b) n_e (LIDAR).

For t = 13 s, figure 19 shows the plasma temperature and density profiles and figure 20 the neutral density both for the bulk plasma and the halo. It must be stressed that in this case, with a high temperature pedestal at the edge, the standard picture of the radial behaviour of the fast neutral source, as shown in figure 10, becomes more complicate, even without taking into

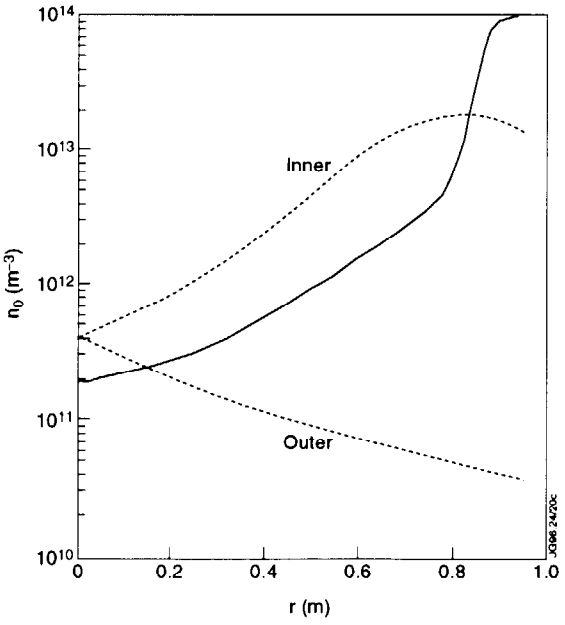

Fig.20: Pulse 32924, t = 13 s; full line: the plasma neutral density, dotted line: the halo neutral density for the inner and outer radial positions along the TOF-NPA line of sight for a neutral beam power of 1 MW.

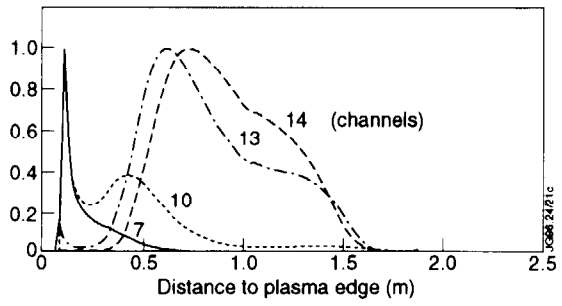

Fig.21: Pulse 32924, t = 13 s; H neutral particle source functions for channels at 14.5 keV, 24.9 keV, 44.5 keV, and 57.3 keV, normalized to their maximua.

account the halo (figure 21). The lower energy neutrals are peaked at the edge, the high energy ones at the centre, and the intermediate energy source function can show a double peak with a very large emission zone. As it was mentioned above, in the case of edge emission the flux and density H/D ratios tend to coincide.

In figure 22 the D and H spectra at 13 s are shown together with two simulation results, the first without the halo effect and the second with a 1 MW neutral beam. Obviously, the high energy D spectrum is dominated by the slowing down ions, and it is not considered in the simulation. The H/D density ratio is 20%. The halo does not affect the low energy channels as the plasma density is rather high, about 4×10^{19} m^{-3}. Moreover, it can be seen that the low H flux at high energy, coming from the plasma centre, is not compatible with even a moderate halo contribution. Therefore, in order to discuss the arguments raised in the previous section, also the case of a radial profile of the H/D density ratio has been evaluated, assuming an exponential decrease from the edge to the centre. The resulting spectra are shown in figure 23 for two cases with 3% H/D at the centre, 20% at the edge with 0.2 m decay length and 25% with 0.1 m, respectively. The assigned neutral beam power is 2 MW and 3 MW, respectively. It can be concluded that the experimental data may be in agreement with a lower H/D ratio in the centre, taking into account the halo contribution.

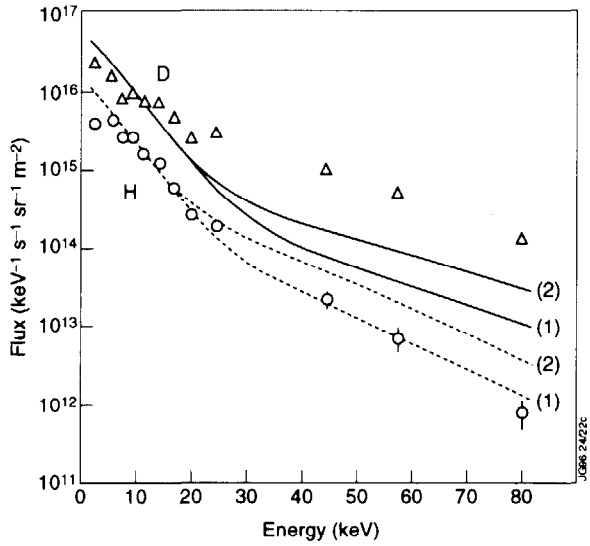

Fig.22: Pulse 32924, t = 13 s; H (O....) and D (Δ —) spectra versus energy. The lines are the model results for (1) no halo, (2) 1 MW halo, n_H/n_D = 20% constant over the radius.

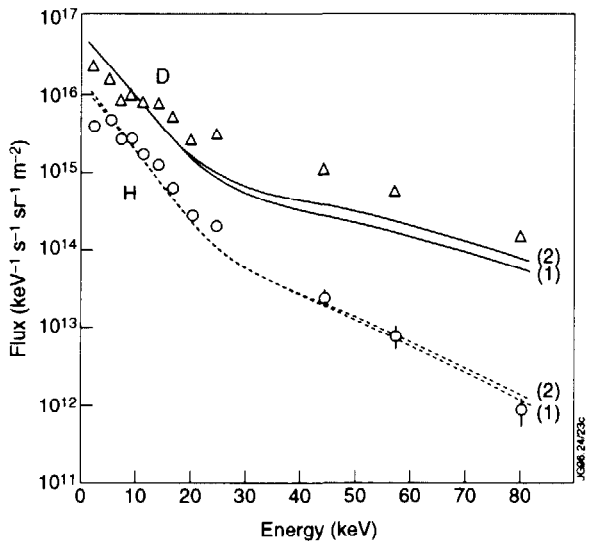

Fig.23: Pulse 32924, t = 13 s; H (O....) and D (Δ —) spectra versus energy. The lines are the model results for a core n_H/n_D = 3% and (1) edge n_H/n_D = 20%, e-folding length 0.2 m, 2 MW halo, (2) edge n_H/n_D = 25%, e-folding length 0.1 m, 3 MW halo.

Figure 24 refers to t = 13.3 s, after the ELM, where a constant H/D density ratio of 3% has been assumed, and the results with a beam power of 2 MW fit the high energy H channels. Again, as at t = 13 s (the density is even higher), only the flux at high energy is affected by the halo.

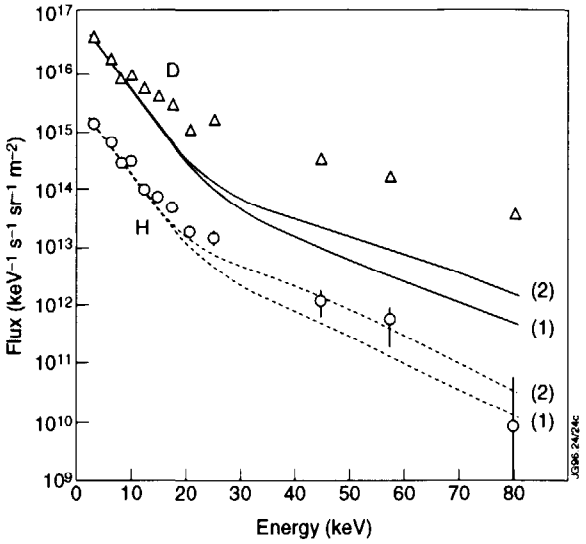

Fig.24: Pulse 32924, t = 13.3 s; H (O....) and D (Δ —) spectra versus energy. The lines are the model results for (1) no halo, (2) 2 MW halo, n_H/n_D = 3% constant over the radius.

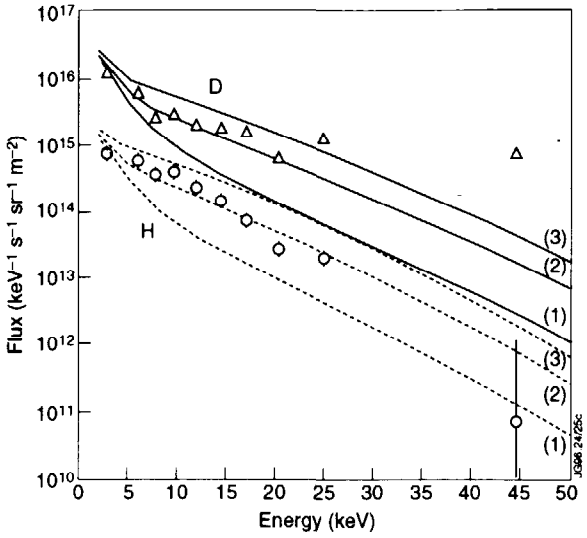

Fig.25: Pulse 32924, t = 12.1 s; H (O....) and D (Δ —) spectra versus energy. The lines are the model results for (1) no halo, (2) 0.7 MW halo, (3) 2 MW halo, n_H/n_D = 5% constant over the radius.

In order to obtain any effect of the halo on the flux at low energy, the density has to be significantly smaller. Figure 25 (t = 12.1 s) refers to a density of 2×10^{19} m^{-3} and shows the results of three simulations without halo and with halo for 0.7 MW and 2 MW beam power, for a density H/D ratio equal to 5%. 0.7 MW appears to fit both spectra, but the main result is that the halo can affect the low energy flux at this density value.

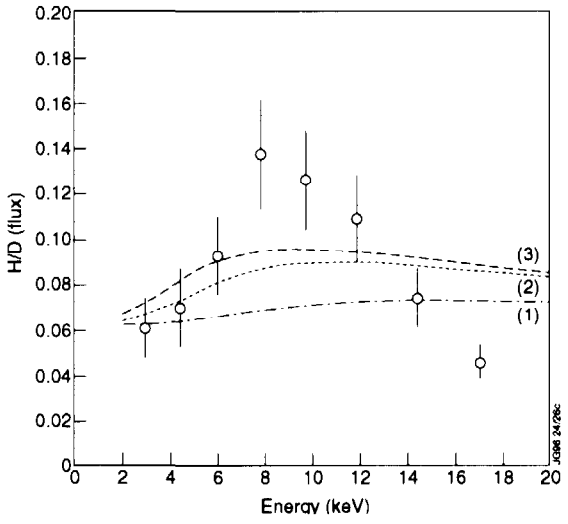

Fig.26: Pulse 32924, t = 12.1 s; experimental H/D flux ratio versus energy, the lines are the model results with n_H/n_D = 5% constant over the radius and (1) no halo, (2) 0.7 MW halo, (3) 2 MW halo.

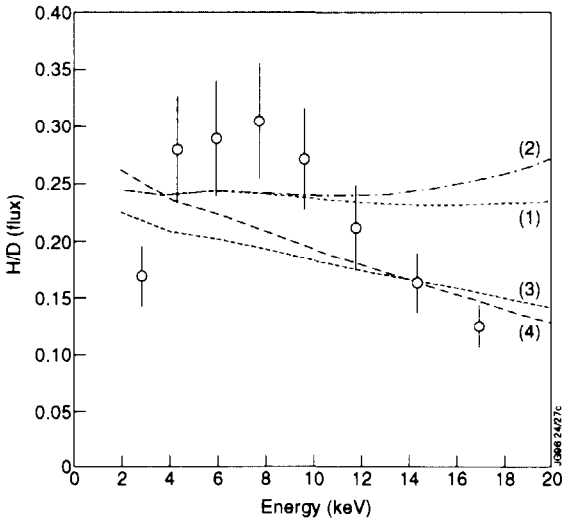

Fig.27: Pulse 32924, t = 13 s; experimental H/D flux ratio versus energy, the lines are the model results with (1,2) n_H/n_D constant corresponding to figure 22 and (3,4) n_H/n_D decreasing towards the plasma centre corresponding to figure 23.

The H/D flux ratio at low energy is shown in figures 26 and 27 for the two cases of low and high density, respectively. In figure 26 the halo is seen to increase the H/D flux ratio, in this case up to 30% for a 2 MW halo, in contrast to figure 27 where only the effects due to the different radial profile assumptions play a role. The low density case, figure 26, demonstrates that the rather fast increase of the H/D ratio at the beam switch on, figure 14 between 12 and 12.5 s, may be attributable to the halo effect. At low density the effect of the halo is mainly to extend the source region, as can be seen in figure 28 where the location of the H neutral particle source is shown as a function of energy, using the same form of presentation as in figure 11. The different attenuation for H and D neutrals gives rise to the variation of the measured H/D flux ratio.

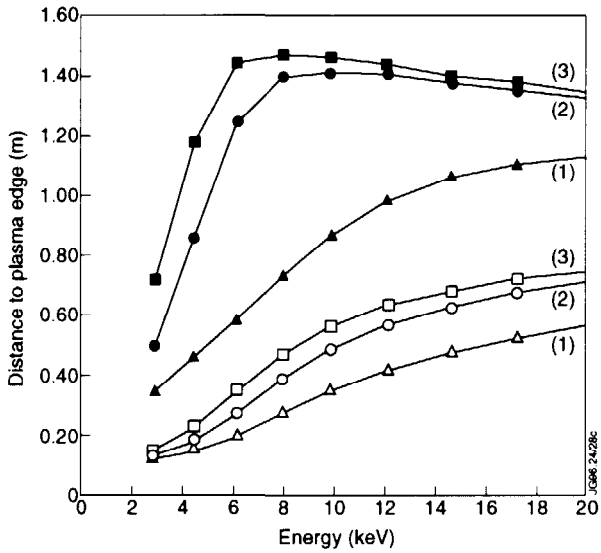

Fig.28: Pulse 32924, t = 12.1 s; distances from the plasma edge up to which 1/6 (open symbols) and 5/6 (full symbols) of the H neutral flux are emitted as a function of energy for (1) no halo, (2) 0.7 MW halo, (3) 2 MW halo.

It must be concluded that the attempt to explain the variation of the H/D flux ratio at low energy by the effect of the beam halo alone has not succeeded at high density, while at low density some minor effects can be expected. The explanation of the observed phenomenon of increase of the H/D flux ratio during the high density ELM-free H mode, and its rapid drop at the ELM, requires more sophisticated modelling, unless it does reflect an actually enhanced H/D density ratio inside the separatrix. A possible candidate is the combination of the halo neutral density and the details of the angular distribution function of the banana orbit ions at their high-field-side tips, which could be influenced by the presence of an ELM-free H mode.

IX. CONCLUSIONS

The measurement of the hydrogen isotope relative concentration by means of the analysis of the emitted flux of neutral particles provides reliable data during the ohmic phase of the plasma. The measured flux ratio must be corrected in order to obtain the proper density ratio because of the different attenuation of the H and D neutrals. An approximate conversion function, applicable to the ohmic phase, has been derived. The typical conversion for JET plasmas consists in a reduction by a factor 2, roughly. The H/D behaviour during part of the 1994-1995 campaign has been studied, and the evolution of the ratio following openings of the vessel and other events has been quantified. The analysis of the ELM-free phase of hot-ion mode plasmas shows interesting features: a large increase of the H/D flux ratio which is quenched, as a rule, by a giant ELM. It has been shown that the phenomenon is at least partially due to a direct beam effect, but the additional neutral density due to the beam and its halo is not sufficient by itself to explain the observation.

ACKNOWLEDGMENT

The authors are grateful to V. Zanza, who is the main author of most of the software package used to evaluate the neutral density including the beam halo effect.

REFERENCES

[1] Afrosimov V V and Petrov M P 1968 Sov. Phys. Tech. Phys. **12** 1467

[2] Afrosimov V V and Kislyakov A J 1982 ISPP, Varenna, "Diagnostics for Fusion Reactor Conditions", EUR 8351-IEN, **1** 289

[3] Wagner F, 1982 J. Vac. Sci. Technol. **20** 1211

[4] Kaita R at al 1985 Nuclear Fusion **8** 939

[5] Corti S, Bracco G, Giannelli A, and Zanza V 1987 Controlled Fusion and Plasma Physics (Proc. 14th Conf. Madrid) European Phys. Society Vol. **II D** 1030

[6] Kaita R et al. 1983 Nuclear Fusion **23** 1089

[7] Giannella R, Zanza V, Barbato E, Bracco G, Corti S, and Gambier D J 1988 Nuclear Fusion **28** 193

[8] Alladio F et al 1984 Nuclear Fusion **24** 725

[9] Horton L D et al 1992 J. Nucl. Mater. **196-198** 139

[10] Bracco G, Betello G, Mantovani S, Moleti A, Tilia B, and Zanza V 1992 Rev. Sci. Instrum. **63** 5685

[11] Bracco G, Corti S, Moleti A, Tilia B, and Zanza V 1991, in ISSP-9, Varenna, "Diagnostics for Contemporary Fusion Experiments" Stott P E, Akulina D K, Gorini G, and Sindoni E (Eds) SIF, Bologna

[12] Gilbody H B 1981 Phys. Scripta **24** 712

[13] Tamor S, 1981 J. Comput. Phys. **40** 104

[14] Simonini R, Taroni A 1986 Controlled Fusion and Plasma Physics (Proc. 13th Conf. Aachen) European Phys. Society Vol. **I** 164

[15] Berezovsky E L et al 1983 Nucl. Fusion **23** 1575

[16] Gordeev Y S 1977 JETP Letters **25** 204

[17] Keilhacker M et al 1990 Phys. Fluids **32** 1291

[18] Azizov E A, Kovan O A, and Mirnov S V, 1993 Proc. 14th Conf. on Plasma Phys. and Contr. Nucl. Fusion Research (Würzburg 1992) IAEA-CN-56/A/A-2-5, Vol.1, IAEA Vienna, 153.